Report

Cell Reports

Loss of *bhlha9* Impairs Thermotaxis and Formalin-Evoked Pain in a Sexually Dimorphic Manner

Graphical Abstract

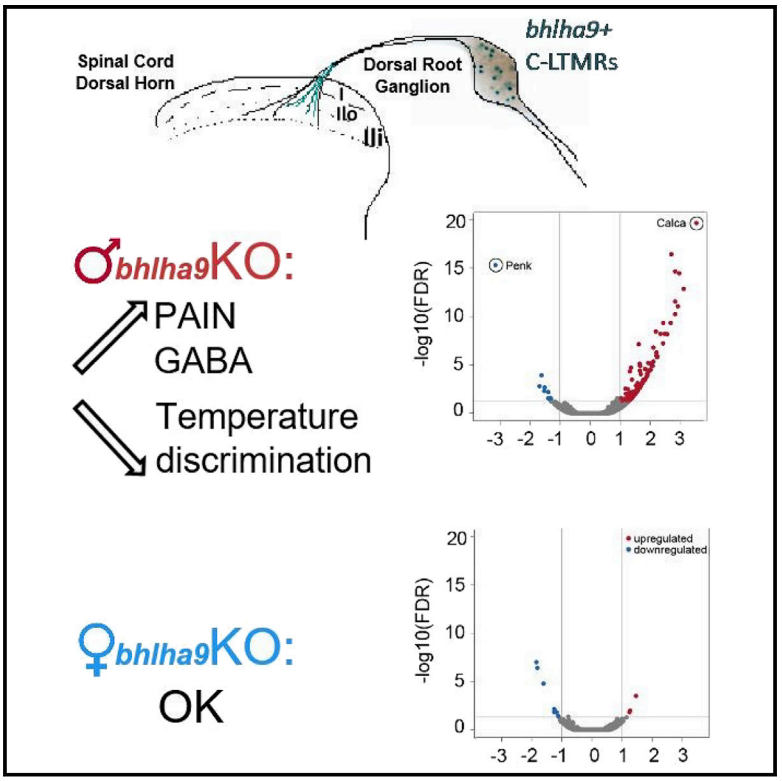

Highlights

- BHLHA9 function in C-LTMRs is sexually dimorphic
- Loss of BHLHA9 impaired formalin-evoked pain selectively in males
- BHLHA9 in C-LTMRs is required for fine discriminative aspects of temperature in males
- Loss of BHLHA9 non-cell-autonomously impairs ionotropic GABAergic signaling

Authors

Manon Bohic, Irène Marics, Catarina Santos, ..., Yves Le Feuvre, Andrew J. Saurin, Aziz Moqrich

Correspondence

aziz.moqrich@univ-amu.fr

In Brief

Bohic et al. demonstrate that mice lacking the transcription factor BHLHA9 exhibit impaired thermotaxis and formalin-evoked pain. BHLHA9 mediates these effects by modulating spinal GABAergic signaling. The data consolidate the role of C-LTRMs in pain sensation and provide *in vivo* evidence of C-LTRMs in the discriminative aspects of temperature sensation.

Bohic et al., 2020, Cell Reports *30*, 602–610
January 21, 2020
https://doi.org/10.1016/j.celrep.2019.12.041

CellPress

OPEN ACCESS
CellPress

Cell Reports
Report

Loss of *bhlha9* Impairs Thermotaxis and Formalin-Evoked Pain in a Sexually Dimorphic Manner

Manon Bohic,[1] Irène Marics,[1] Catarina Santos,[1] Pascale Malapert,[1] Nissim Ben-Arie,[2,6] Chiara Salio,[3,6] Ana Reynders,[1,6] Yves Le Feuvre,[4,5,6] Andrew J. Saurin,[1,6] and Aziz Moqrich[1,7,*]

[1]Aix-Marseille Université, CNRS, Institut de Biologie du Développement de Marseille, UMR 7288, Case 907, 13288 Marseille, Cedex 09, France
[2]Department of Cell and Developmental Biology, Institute of Life Sciences, Edmond J. Safra Campus at Givat-Ram, The Hebrew University of Jerusalem, Jerusalem 9190401, Israel
[3]Department of Veterinary Sciences, University of Turin, 10095 Grugliasco (TO), Italy
[4]University of Bordeaux, Interdisciplinary Institute for Neuroscience, UMR 5297, 33000 Bordeaux, France
[5]CNRS, Interdisciplinary Institute for Neuroscience, UMR 5297, 33000 Bordeaux, France
[6]These authors contributed equally
[7]Lead Contact
*Correspondence: aziz.moqrich@univ-amu.fr
https://doi.org/10.1016/j.celrep.2019.12.041

SUMMARY

C-LTMRs are known to convey affective aspects of touch and to modulate injury-induced pain in humans and mice. However, a role for these neurons in temperature sensation has been suggested, but not fully demonstrated. Here, we report that deletion of C-low-threshold mechanoreceptor (C-LTMR)-expressed *bhlha9* causes impaired thermotaxis behavior and exacerbated formalin-evoked pain in male, but not female, mice. Positive modulators of $GABA_A$ receptors failed to relieve inflammatory formalin pain and failed to decrease the frequency of spontaneous excitatory post-synaptic currents (sEPSCs) selectively in *bhlha9* knockout (KO) males. This could be explained by a drastic change in the GABA content of lamina II inner inhibitory interneurons contacting C-LTMR central terminals. Finally, C-LTMR-specific deep RNA sequencing revealed more genes differentially expressed in male than in female *bhlha9* KO C-LTMRs. Our data consolidate the role of C-LTMRs in modulation of formalin pain and provide *in vivo* evidence of their role in the discriminative aspects of temperature sensation.

INTRODUCTION

The somatosensory nervous system is key to our daily interactions with the outside world, mental well-being, and survival. It allows us to feel changes in our body as well as external stimulations, from a sprained ankle to the relaxing effect of a massage. The somatosensory neurons that innervate our skin are responsible for the detection of those stimuli and the transmission of the signal to the spinal cord (SC), a gate that normally allows only relevant information to be sent to higher structures. However, a defect anywhere in this chain of information can lead to chronic pain, a life-disrupting condition that affects 20% of the population in the world.

Somatosensory neurons are highly heterogeneous, to par with the wide array of sensations they allow us to detect. As such, they can be subdivided into distinct populations according to not only their anatomy, physiology, and the modalities they detect but also their molecular profile. A good knowledge of this molecular identity is key to understanding the specificities of each population and to developing appropriate genetic tools to study them. Even though somatosensory neurons have been the subject of studies for decades now, one particular subpopulation of neurons called C-low-threshold mechanoreceptors (C-LTMRs) has only recently been at the forefront of sensory and pain research. These hairy-skin innervating neurons are highly conserved across species (Seal et al., 2009; Vallbo et al., 1999; Zotterman, 1939). They mediate affective touch (Löken et al., 2011) and modulate pain in mouse and human (Delfini et al., 2013; Francois et al., 2015; Liljencrantz and Olausson, 2014; Nagi et al., 2011; Urien et al., 2017). Interestingly, they are also activated by cooling (Li et al., 2011). Few studies hint at the spinal circuitry that could explain such a duality: transduction of innocuous sensation and pain modulation (Kambrun et al., 2018).

Here, we take advantage of the C-LTMR molecular repertoire recently generated in our laboratory (Reynders et al., 2015) to show that the transcription factor *bhlha9* is highly enriched in this population compared to the rest of the nervous system. Its expression appearing only after birth makes it an interesting genetic tool to study C-LTMR function. Male, but not female, mice lacking BHLHA9 show a wide-ranging thermotaxis defect compared to littermate controls. Moreover, the same male mice present an exacerbated inflammatory pain in the formalin test paradigm. This exacerbated pain is insensitive to the normally analgesic effect of $GABA_A$ receptor positive modulation, suggesting that loss of *bhlha9* impairs the ionotropic GABAergic signaling in a sexually dimorphic manner. Blind recording of interneurons located in lamina II inner of dorsal horn SC (the spinal region receiving C-LTMRs inputs) shows that NS11394-mediated decrease of the frequency of spontaneous excitatory post-synaptic currents (sEPSCs) was selectively impaired in *bhlha9* knockout (KO) males. Furthermore, using immuno-electron microscopy experiments, we found an intriguing increase in GABA content in GABAergic interneurons selectively in *bhlha9* KO males. Finally, transcriptomic analysis of

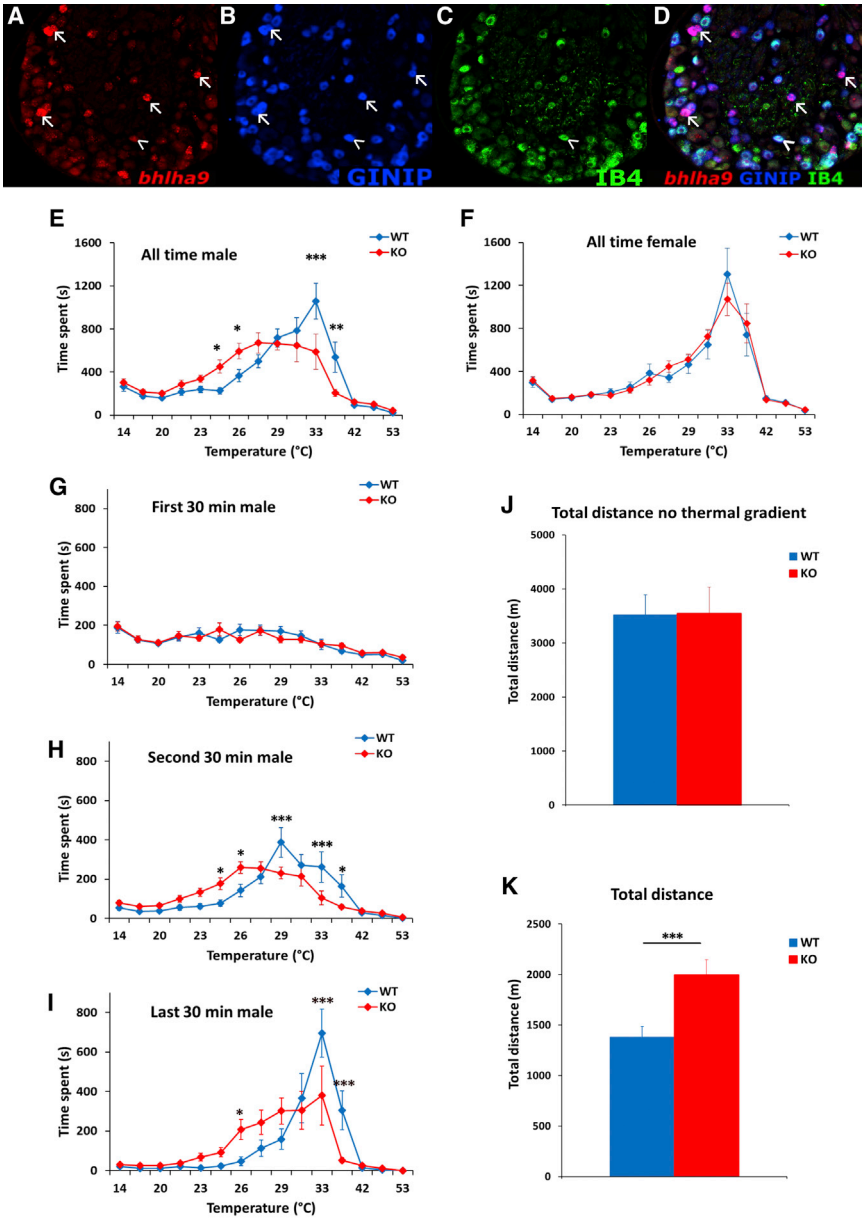

Figure 1. *bhlha9* Is Highly Expressed in C-LTMRs, and Loss of Function of *bhlha9* Affects Temperature Perception in Male, but Not Female, Mice

(A) *In situ* hybridization for *bhlha9* on a thoracic DRG section. (B) Immunostaining using anti-GINIP antibody (C) IB4 binding. (D) Overlay of the three stainings.⁻ Arrows indicate *bhlha9*$^+$ C-LTMRs (A, B, and D), and the arrowhead indicates a low *bhlha9* expressor GINIP$^+$ IB4$^+$ neuron known as MrgprD$^+$ neuron (A–D).

(E) Overall behavior of WT and *bhlha9* KO male mice (WT n = 16, KO n = 13).

(F) Overall behavior of WT and *bhlha9* KO female mice (WT n = 16, KO n = 17).

(G–I) Behavior of WT and *bhlha9* KO male mice during the first (G), second (H), and last (I) 30 min of the gradient test.

(J and K) Total distance traveled by male mice when the floor of the thermotaxis apparatus is set at room temperature (WT n = 9, KO n = 9) and total distance traveled during the thermotaxis test (K).

The statistical tests used were a two-way ANOVA for (A)–(E) and a one-way ANOVA for (F) and (G); *p < 0.05, ***p < 0.001.

RNA contents extracted from fluorescence-activated cell sorting (FACS)-sorted C-LTMRs of male and female wild-type (WT) and *bhlha9* KO mice showed that loss of function of bhlha9 leads to stronger gene dysregulation in males than females, further supporting the sexually dimorphic effects observed in our behavioral, electrophysiological, and ultrastructural experiments.

RESULTS

bhlha9 Is Dispensable for DRG Neuron Survival, Maturation, and Target Innervation

Recent studies using RNA deep sequencing on single and sorted primary sensory neurons revealed the transcription factor *bhlha9* among the few markers highly enriched in adult C-LTMRs (Reynders et al., 2015; Reynders and Moqrich, 2015; Usoskin et al., 2015). Triple staining experiments using *bhlha9* RNA probe in combination with galpha inhibitory interacting protein (GINIP) antibody (Gaillard et al., 2014) and IB4 binding demonstrated that *bhlha9* is expressed exclusively in GINIP$^+$ neurons; more specifically, the great majority of them are GINIP$^+$/IB4$^-$ neurons, which represent C-LTMRs (Figures 1A–1D). Quantification analysis showed that *bhlha9* is expressed in 11% of total dorsal root ganglia (DRG) neurons and that high expression occurs in 60% of GINIP$^+$/IB4$^-$ C-LTMRs and low expression occurs in 6% of GINIP$^+$/IB4$^+$ neurons (Figures S1A). RT-qPCR experiments showed that the highest expression of *bhlha9* in the nervous system occurs in DRG neurons (Figure S1B). It starts just after birth and reaches adult levels by post-natal day 20 (Figure S1C).

To gain insight into the role of *bhlha9* in sensory physiology, we took advantage of *bhlha9* KO mice previously generated and characterized by Schatz and colleagues (Schatz et al., 2014).

We first validated *bhlha9* loss of expression in the DRG of *bhlha9* KO mice using *in situ* hybridization for *bhlha9* in combination with GINIP immunostaining and isolectin binding 4 (IB4) binding (Figures S1D–S1G). Quantification of *Ret*-, *TrkA*-, *TrkB*-, TrkC-, GINIP$^+$/IB4$^+$-, and GINIP$^+$/IB4$^-$-expressing neurons showed no difference between *bhlha9* KO and their WT littermates (Figure S1H). To visualize the peripheral projections of

C-LTMRs, we used GINIP immunostaining on whole mount hairy skin using the clearing method (Li et al., 2011). GINIP$^+$ C-LTMR axonal branches form the same types of longitudinal lanceolate endings around hair follicles in both genotypes (Figures S1I and S1J). To visualize the central projections of C-LTMRs, we first performed a series of triple staining experiments on SC sections using antibodies against CGRP, GINIP, and PKCγ in combination with IB4 binding. We found that peptidergic CGRP$^+$ fibers mainly innervate lamina I, the cutaneous non-peptidergic GINIP$^+$/IB4$^+$ afferents invade outer lamina II and C-LTMRs GINIP$^+$/IB4$^-$ terminals project to the most inner part of lamina II, where they overlap with the PKCγ^+ interneurons (Figures S1K–S1N). These data demonstrate that loss of BHLHA9 has no effect on the gross anatomy of C-LTMRs. To further confirm this observation, we performed ultrastructural quantitative analysis specifically targeting type Ia (GIa) glomeruli in lamina II inner. We applied the same strategy described by Kambrun et al. 2018 in a study using antibodies against GINIP and VGLUT3 in order to distinguish C-LTMRs central terminals from those of other C-fibers invading lamina II inner of the SC. Under these conditions, GINIP$^+$/VGLUT3$^+$ GIa glomeruli are C-LTMRs, GINIP$^+$/VGLUT3$^-$ represent the cutaneous C-fibers, and the double-negative GINIP$^-$/VGLUT3$^-$ correspond to other C-fiber types. Quantification analyses show no difference in the distribution of the three types of GIa profiles as well as in their density between WT and *bhlha9* KO mice of both genders (Figures S1O–S1R and S3M–S3X). Taken together, these results demonstrate that BHLHA9 is dispensable for the survival, maturation, and anatomical organization of C-LTMRs.

Thermotaxis Is Impaired in *bhlha9* KO Male, but Not Female, Mice

Since their discovery by the Swedish physiologist (Zotterman, 1939), the role of C-LTMRs in conveying hedonic aspects of touch is well established. However, the role of these neurons in other somatosensory sensations is under intense investigation. To gain insight into the role of *bhlha9* in temperature sensation, we subjected *bhlha9* KO male and female mice to a large battery of temperature tests. We found no difference between WT and *bhlha9* KO mice in the hot and cold plate (Figures S2A–S2D) as well as in the two-temperature choice tests (Figures S2E–S2H). However, in the temperature gradient paradigm, male mice exhibited a net shift toward cooler temperatures in comparison to their WT littermates, whereas *bhlha9* KO female mice displayed the same thermotaxis behavior as the WT mice (Figures 1E and 1F). Indeed, when we break down the behavior of the male mice into three consecutive 30 min, one can see that during the first 30 min, *bhlha9* KO males exhibited the same exploratory behavior as their WT littermates (Figure 1G). During the second 30 min, WT mice started to show a clear bias toward the warmer area of the arena, whereas *bhlha9* KO males occupy a much wider area with a bias toward cooler temperatures (Figure 1H). This behavior is strongly reinforced during the last 30 min, with WT mice showing a strong preference of ~33°C and *bhlha9* KO male mice seemingly unable to make a difference between temperatures ranging from 24°C to 37°C (Figure 1I), suggesting that temperature sensation is impaired in *bhlha9* KO male mice. To test whether this phenotype is due to impaired temperature sensation or perturbed locomotor activity in *bhlha9* KO male mice, we measured the total distance traveled by WT and *bhlha9* KO male mice under two conditions: (1) when the floor temperature of the arena was set at room temperature, and (2) when the floor temperature was subjected to a gradient varying from 15°C to 55°C (Figures 1J and 1K). We found that WT and *bhlha9* KO male mice traveled the same distance during the 90-min period when the floor temperature was set at room temperature (Figure 1J), demonstrating normal locomotor activity of *bhlha9* KO male mice. However, when the temperature gradient was set between 15°C and 55°C, *bhlha9* KO male mice traveled a much longer distance than their WT littermates (Figure 1K), demonstrating that loss of BHLHA9 impairs the ability of *bhlha9* KO mice to adapt their behavior to a change in temperature, further supporting a potential role of C-LTMRs in discriminative aspects of temperature sensation.

Formalin-Evoked Pain Is Exacerbated in *bhlha9* KO Male, but Not Female, Mice

Recent studies in humans and rodents provided evidence that C-LTMRs also play a role in modulation of injury-induced mechanical and chemical pain (Delfini et al., 2013; Francois et al., 2015; Kambrun et al., 2018; Liljencrantz and Olausson, 2014; Nagi et al., 2011; Urien et al., 2017). Given the enriched expression of *bhlha9* in C-LTMRs, we first tested gross innocuous mechanical sensitivity of *bhlha9* KO mice using the tape test (Figures S2I–S2L). We found no significant difference between the two genotypes, suggesting that loss of BHLHA9 is dispensable for C-LTMRs to sense light-touch stimuli. We then tested the mechanical and thermal sensitivity of *bhlha9* KO mice under acute and two different pathological conditions: the chronic constriction injury of the sciatic nerve (CCI) (Bennett and Xie, 1988) and carrageenan-induced inflammation. In both neuropathic and inflammation-induced pain paradigms, mechanical thresholds at baseline and at all the time points tested after injury were similar in WT and *bhlha9* KO mice (Figures S2M and S2N). Furthermore, *bhlha9* KO mice had the same responses to noxious cold stimuli before and after CCI and displayed the same Carrageenan-induced thermal hypersensitivity in the Hargreaves test (data not shown). Taken together, our results show that BHLHA9 is dispensable for acute and injury-induced mechanical and thermal hypersensitivity.

Previous studies from our laboratory demonstrated that C-LTMRs play a critical role in modulation of formalin-evoked pain (Delfini et al., 2013; Urien et al., 2017). To test whether loss of BHLHA9 affects the ability of *bhlha9* KO mice to sense chemical pain, we subjected them to the formalin test. As shown in Figures 2A–2D, intraplantar injection of 2% formalin triggers robust first and second pain responses in males and females of both genotypes. *bhlha9* KO male, but not female, mice exhibited an exacerbated pain response to formalin injection during the second phase, suggesting a sexually dimorphic enhanced central sensitization in these mice (Figures 2A and 2B).

Previous studies have shown that the ionotropic GABAergic signaling plays a critical role in modulation of formalin-evoked pain (Munro et al., 2011). We also showed that the C-LTMR-derived TAFA4 modulated injury-induced pain through activation

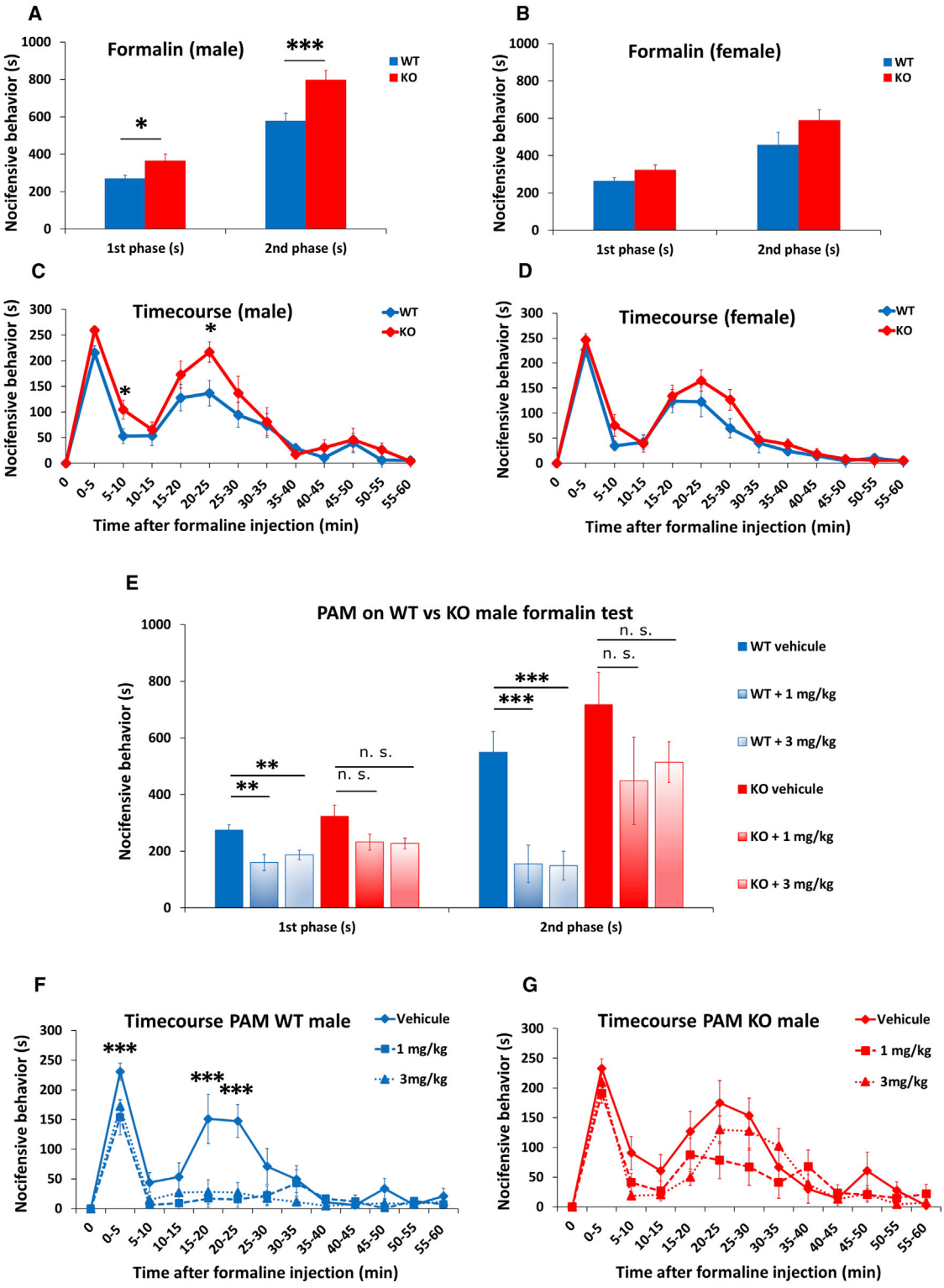

Figure 2. *bhlha9* KO Male, but Not Female, Mice Exhibit PAM-Insensitive Exacerbated Chemical Pain in the Formalin Test during Both the First and the Second Phase

(A) Nocifensive behavior of WT and *bhlha9* KO male mice during the first and the second phase of the formalin test (WT n = 13, KO n = 12).

(B) Nocifensive behavior of WT and *bhlha9* KO female mice during the first and the second phase of the formalin test (WT n = 12, KO n = 17).

(C) Time course of the nocifensive response of WT and *bhlha9* KO male mice during the formalin test.

(legend continued on next page)

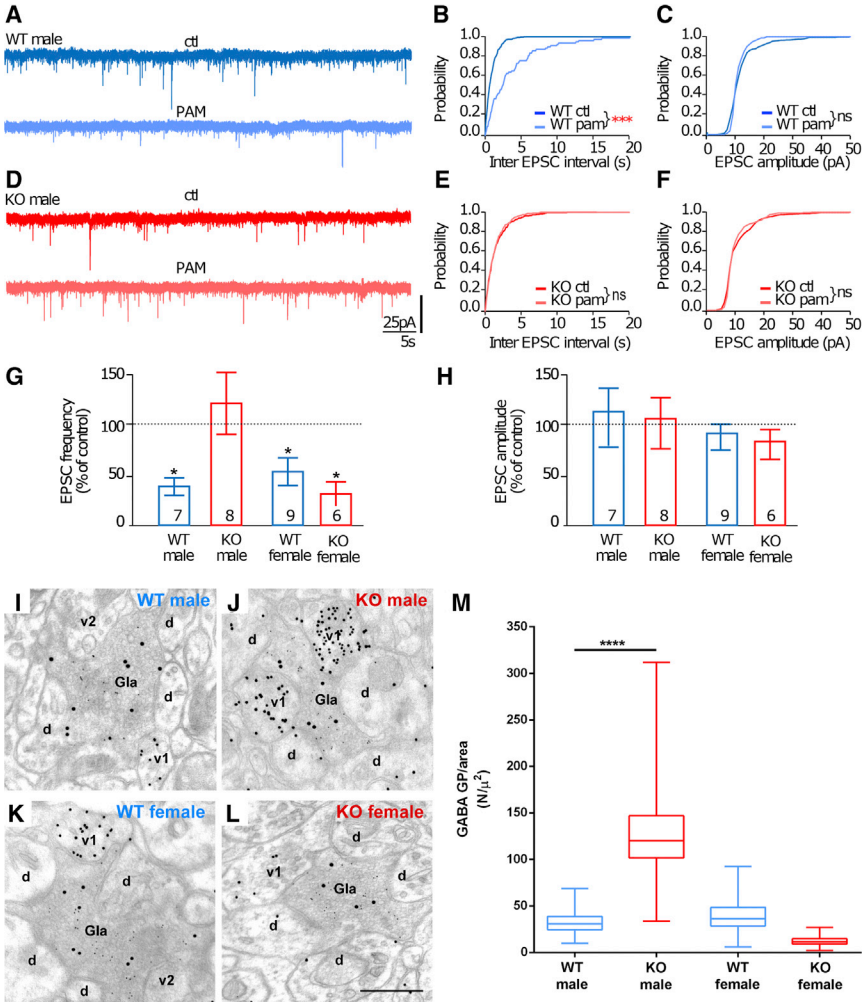

Figure 3. Loss of Function of *bhlha9* Leads to Increased EPSC Frequency and GABA Expression in Lamina II Inner Neurons in Male Mice Only

(A–C) Voltage-clamp recordings (A), frequency (B), and amplitude (C) distribution of spontaneous excitatory synaptic currents (sEPSCs) in a lamina II inner neuron of a WT male animal, before and during superfusion of NS11394.

(D–F) Voltage-clamp recordings (D), frequency (E), and amplitude (F) distribution of sEPSCs for a lamina II inner neuron of a *bhlha9* KO male animal before and during superfusion of NS11394.

(G and H) Variation of EPSC frequency (G) and amplitude (H) in males and females of both genotypes. *$p < 0.05$.

(I–L) Examples of GINIP$^+$/VGLUT3$^+$ C-LTMR central terminals, organized in non-peptidergic glomeruli of the type Ia (Gla) in WT males (I), WT females (J), *bhlha9* KO males (K), and *bhlha9* KO females (L), in synaptic contact with GABA-immunolabeled vesicle-containing dendrites (V1). Scale bar, 500 nm.

(M) Box chart showing GABA gold particle (GP) densities in V1 profiles (GABA GP/area, N/μ2) in WT and *bhlha9* KO male and female mice. Very high levels of GABA are present in *bhlha9* KO males, low levels of GABA are present in *bhlha9* KO females, and normal levels are found in WT males and females (Mann-Whitney test, $p < 0.0001$).

Loss of BHLHA9 Non-Cell-Autonomously Affects Spinal Transmission, Likely through Impaired GABA Content in GABAergic Interneurons

of GABAergic transmission (Kambrun et al., 2018). Given that *bhlha9* KO male mice exhibited a much higher pain response to formalin, we hypothesized that this formalin-evoked hypersensitivity could be due to an impaired ionotropic GABAergic signaling in these mice. To test this, 30 min prior to formalin injection, WT and *bhlha9* KO male mice received an oral administration of the positive allosteric modulator of the ionotropic GABAergic signaling NS11394 known for its pain relief effect during formalin inflammation in the rat (Munro et al., 2011). We found that 1 and 3 mg/kg NS11394 provided a significant pain relief during both phases of formalin-evoked pain in WT mice (Figures 2E and 2F). However, both doses had virtually no effect in *bhlha9* KO male mice (Figures 2E and 2G), demonstrating that loss of BHLHA9 exacerbates formalin-evoked pain through a dysfunction of the ionotropic GABAergic system selectively in male mice.

To assess whether the sexually dimorphic deficits in nocifensive behavior were mirrored by selective alterations in spinal neurons physiological properties, we recorded unidentified lamina II inner neurons (WT male: n = 20; *bhlha9* KO male: n = 23, WT female: n = 9, and *bhlha9* KO female: n = 8) from spinal slices of juvenile mice. Recorded neurons were characterized for their intrinsic passive and active properties (Figures S3A and S3B). We found no differences among the four experimental groups in all parameters tested (one-way ANOVA; Figures S3C–S3I). Similarly, the average frequency, amplitude, and decay of sEPSCs recorded in lamina II inner neurons did not differ significantly among the four groups (Figures S3J–S3L). As *bhlha9* deletion results in a loss of sensitivity to NS11394 in the formalin test, we examined the effects of NS11394 superfusion on sEPSC firing in WT and *bhlha9* KO animals. In WT males, NS11394 induced a significant decrease of sEPSC frequency in 6 out of 7 recorded neurons

(D) Time course of the nocifensive response of WT and *bhlha9* KO female mice during the formalin test.

(E) Nocifensive behavior of WT and *bhlha9* KO male mice during the formalin test following per os administration of NS11394, positive allosteric modulator (PAM) of $GABA_A$ receptors at 1 or 3 mg/kg, or its vehicle.

(F and G) Time course of the nocifensive response of WT (F) and *bhlha9* KO (G) male mice during the formalin test following per os administration of NS11394.

The statistical tests used were a two-way ANOVA for (C), (D), (F), and (G) and a one-way ANOVA for (A), (B), and (E); *$p < 0.05$, **$p < 0.01$, ***$p < 0.001$.

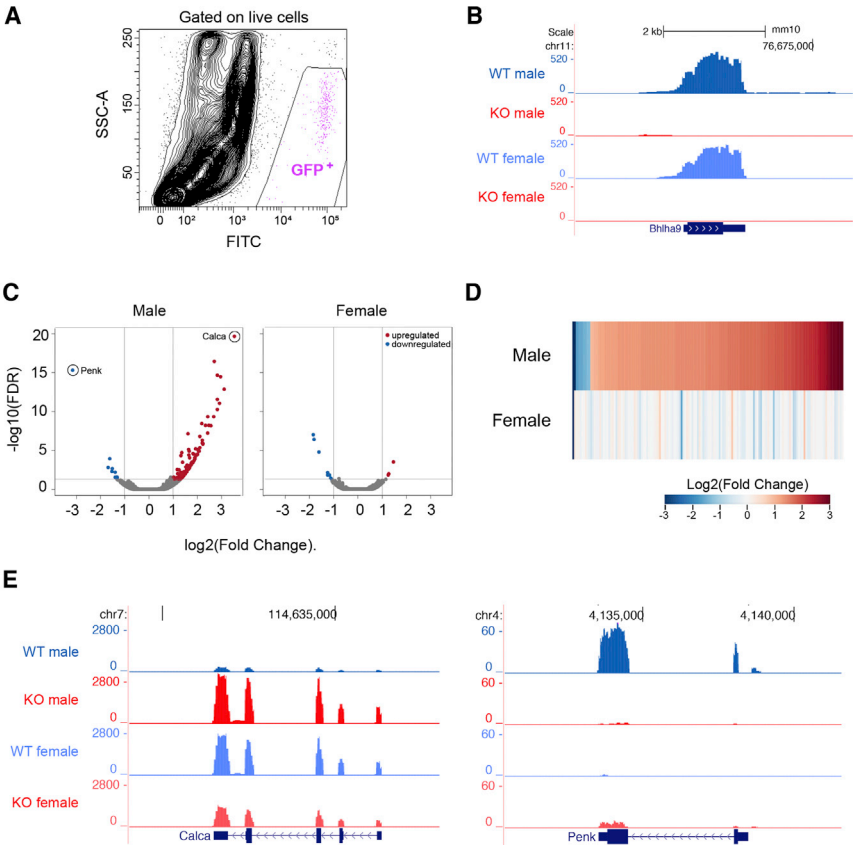

Figure 4. Loss of Function of *bhlha9* Leads to a Striking Change in the Molecular Profile of C-LTMRs, Specifically in Male Mice

(A) Representative FACS dot-plot illustrating the gating strategy for C-LTMRs sorting using Tafa4$^{venus/+}$ mouse model. Dead cells were excluded and GFP^{+} C-LTMRs were sorted from WT::Tafa4$^{venus/+}$ and bhlha9 KO::Tafa4$^{venus/+}$ male and female mice. The GFP^{+} population represented 0.1% of live cells in each genotype and gender.

(B) Genome browser track of reads per kilo base per million mapped reads (RPKM)-normalized RNA-sequencing reads mapping to the *bhlha9* gene shows *bhlha9* expression in WT male and female mice, but no expression in *bhlha9* KO mice.

(C) Volcano plots showing the 148 differentially expressed genes (DEGs) in male mice and 12 DEGs in female mice upon bhlha9 KO. Note that bhlha9 is not represented on the plots due to the small false discovery rate (−log10 value of 145).

(D) Heatmap representation of the 148 male DEGs with the corresponding fold change values, irrespective of significance, in female C-LTMRs shows little variation in expression in females upon *bhlha9* KO.

(E) Genome browser tracks of RPKM-normalized RNA-sequencing reads of the highly overexpressed (Calca) and repressed (Penk) genes highlight the sexually dimorphic expression traits of *bhlha9* KO in male C-LTMRs.

(Kolmogorov-Smirnov [KS] test, $p < 0.05$; Figures 3A and 3B). However, in *bhlha9* KO males, NS11394 had no effect on EPSC frequency in 6 out of 8 recorded neurons (Figures 3D and 3E). NS11394 had no effect on EPSC amplitude in males and females of both genotypes (Figures 3C and 3F). In line with the behavioral data, lack of effect of NS11394 was only observed in *bhlha9* KO male animals, as NS11394 induced a significant decrease in EPSC frequency in both WT and *bhlha9* KO females (n = 7 neurons out of 9 and n = 7 out of 7, respectively). Indeed, NS11394 induced a significant decrease in average EPSC frequency in WT male (−61% + −8.7%), WT females (−47% + −12.57%), and *bhlha9* KO females (70% + −12.30%), but not in *bhlha9* KO males (Figure 3G). NS11394 had no effect on average EPSC amplitude in all four groups (Figure 3H). Taken together, these data demonstrate that loss of BHLHA9 causes a male-specific impairment of the ionotropic GABAergic signaling.

To assess the mechanisms underlying the impaired response of *bhlha9* KO males to the positive modulation of NS11394, we performed multiple immunoelectron microscopy (immuno-EM) experiments to quantify the GABA content in vesicle-containing dendrites (V1) originating from GABAergic interneurons and contacting C-LTMR central terminals (Gla glomeruli) in WT and *bhlha9* KO mice of both genders. Here again, quantitative analysis revealed a selective bias toward *bhlha9* KO males (Figures 3I–3M). Indeed, WT male and female mice showed roughly similar degree of GABA content in their V1 profiles (31.99 gold particles GPs/μ^2 in males versus 38.93 GPs/μ^2 in females). However, *bhlha9* KO male mice showed a very high level of GABA immunolabeling (126.89 GPs/μ^2), whereas female mice showed a slight decrease in GABA immunolabeling (12.23 GPs/μ^2).

Loss of BHLHA9 Affects Gene Expression in C-LTMRs in a Sexually Dimorphic Manner

To further assess the molecular mechanisms underlying the sexually dimorphic phenotypes in *bhlha9* KO mice, we performed whole-genome RNA sequencing on FACS-sorted C-LTMRs. To do so, we crossed *bhlha9* KO mice with TAFA4$^{venus/+}$ mice (Delfini et al., 2013) to genetically mark C-LTMRs in a WT and in a *bhlha9* KO background. Using the same strategy described previously (Reynders et al., 2015; Reynders and Moqrich, 2015) we FACS-sorted Venus-expressing C-LTMRs of adult WT and *bhlha9* KO mice of both genders (Figure 4A). High-quality RNA was extracted and submitted to RNA deep sequencing technology in order to generate their respective transcriptional profiles. Sequences were mapped to the mm10 UCSC mouse genome assembly resulting in 91%–93% correctly mapped reads, which were used for differential gene expression analyses. We first demonstrated that the FACS-sorted neurons were indeed C-LTMRs by checking the expression of specific markers such as tyrosine hydroxylase (TH), VGLUT3 (Slc17a8), and TAFA4 (Figure S4A). We next

demonstrated that *bhlha9* transcripts were expressed at the same levels in male and female WT and that this expression was abolished in *bhlha9* KO C-LTMRs in both genders (Figure 4B). To identify differentially expressed (DE) genes between WT and *bhlha9* KO C-LTMRs, we used DESeq2 (Love et al., 2014) (version 1.14.1) using a false discovery rate (p-adjusted value in DESeq2) threshold of 0.05 and at least a two-fold change in expression. Remarkably, we found that loss of BHLHA9 had a much stronger effect in males than in females C-LTMRs. Indeed, 147 genes were found to be DE in male C-LTMRs in comparison to only 11 DE genes in females (Figures 4C–4E; Table S1). Interestingly, out of the 147 male DE genes, 138 were upregulated (93%) and only 9 were downregulated (7%). In contrast, among the 11 female DE genes, 3 (28%) were upregulated and 8 (72%) were downregulated (see Table S1). An example of such differential expression occurring in opposite direction in males versus females is shown in Figure S4B. One can see that in the WT context, *Faim2* and *Gpx3* genes are almost silent in male, but not female, WT, whereas in the *bhlha9* KO context, *Faim2* and *Gpx3* genes are upregulated in males but downregulated in females. Taken together, the transcriptomic data provide an additional demonstration that BHLHA9 functions in a sexually dimorphic manner in mouse C-LTMRs.

DISCUSSION

In this study, we report the identification of *bhlha9* as a novel marker of C-LTMRs and demonstrate that male mice lacking this transcription factor exhibit two major phenotypes: (1) a temperature-sensation defect mainly revealed by the incapacity of the mutant mice to finely tune their thermotaxis behavior and (2) an exacerbated response to formalin-evoked pain. Both phenotypes could be explained by an impaired ionotropic GABAergic signaling convincingly supported by electrophysiological and ultrastructural data. In addition, we provide transcriptomic data demonstrating that BHLHA9 functions in mouse C-LTMRs in a sexually dimorphic manner.

C-LTMRs have been proposed to play a key role in temperature sensation. *In vitro* recordings show that C-LTMRs can fire in response to cooling, both during skin-nerve experiments (Zimmermann et al., 2009) with a response to decreases in temperature ranging from 50°C to 30°C and from 30°C to 2°C (Li et al., 2011) and in cultured primary sensory neurons (Francois et al., 2015). The wide-ranging thermotaxis defect exhibited by *bhlha9* KO mice is reminiscent of this wide-ranging activation of C-LTMRs by cooling. The *bhlha9* KO mice defect encompasses almost the whole range of innocuous temperatures (Figure 1; 24°C to 37°C) and underlines a possible deficiency in sensing a variation in temperature, but not detection of specific temperatures. This observation is supported by the fact that *bhlha9* KO animals still correctly avoid noxious heat and cold temperatures as highlighted in Figure S2. This C-LTMR thermosensitivity is quite intriguing, because it is vastly different from other thermosensitive fibers characterized by a defined thermal threshold of activation, set for example by the types of Transient Receptor Potential (TRP) ion channels they express.

The actual molecular mechanism responsible for C-LTMR sensitivity to cooling is still unknown, but there may be an evolutionary explanation. This characteristic response to cooling is conserved across species, with human C-LTMRs, called C-tactile or CT afferents, displaying similar properties (Nordin, 1990). Indeed, human studies show that CT temperature and mechanical activation are tightly linked. People perceive gentle touch, such as caress, as more pleasant when it is delivered at skin temperature, 32°C, rather than at a cooler or a warmer temperature (18°C or 42°C). Remarkably, this heightened pleasantness of touch correlates with C-LTMR maximal firing frequency (Ackerley et al., 2014). Hence, one hypothesis could be that C-LTMRs are optimally tuned to detect and transduce affective social touch, both in terms of thermal and mechanical parameters. And their thermal sensitivity would have more of a social and hedonic valence than other sensory-discriminative thermosensitive fibers.

We also found that *bhlha9* KO male mice exhibited an exacerbated formalin pain during the second phase. Behavioral pharmacology demonstrated that the interphase and the magnitude of the second phase are tightly controlled by the spinal GABAergic system (Kaneko and Hammond, 1997). For example, it has been shown that intrathecal (IT) injection of bicuculline increases pain behavior during the interphase and the second phase without affecting the first phase. In contrast IT administration of muscimol or isoguvacine produced a significant decrease of both phases (Kaneko and Hammond, 1997). Given that *bhlha9* KO male mice exhibited an enhanced formalin pain during the second phase, we hypothesized that this phenotype was due to an impaired spinal GABAergic signaling. To test this hypothesis, we transposed to the mouse the experiment performed in the rat by Munro and colleagues (Munro et al., 2011). Two different doses of NS11394 (1 and 3 mg/kg) provided a highly significant pain relief for WT male mice during the first and the second phase (Figure 2). However, there was no significant anti-nociceptive effect in *bhlha9* KO mice during either phase. To provide a mechanistic explanation of the male-specific phenotype, we used electrophysiology on SC slice. We showed that NS11394 failed to decrease the frequency of sEPSCs only in *bhlha9* KO males, supporting the selective absence of NS11394-mediated pain relief in these mice. We next used immuno-EM experiments and showed a selective and drastic increase in GABA content in the V1 terminals of GABAergic interneurons in synaptic contact with GIa located in laminae II inner of *bhlha9* KO male mice. Could this GABA increase in V1 terminals of GABAergic interneurons explain the impaired response of *bhlha9* KO males to the analgesic effect of NS11394?

Two possible explanations are that (1) higher levels of GABA in V1 terminals lead to increased release and desensitization of spinal $GABA_A$ receptors, mimicking the phenomenon of loss of inhibition, known to occur in a variety of pathological conditions. This is unlikely, because *bhlha9* KO male mice showed no signs of mechanical allodynia, which is a hallmark of loss of inhibition. Furthermore, *bhlha9* KO male mice behaved the same way as their WT littermates in the setting of inflammation and neuropathic pain conditions (Figure S2). (2) Higher levels of GABA in V1 terminals lead to increased release of GABA on primary afferent central projections, leading to the so-called enhanced primary afferent depolarization (PAD). Thus, the inhibitory function of GABA on primary afferent neurons will be shifted into a net excitation. Under these conditions, positive modulation of

$GABA_A$ receptors by NS11394 would fail to exert its pain relief effect.

What triggers the male-specific increase of GABA contents in V1 terminal of lamina II inner GABAergic interneurons? Our transcriptomic analyses showed that loss of BHLHA9 leads to stronger gene dysregulation in males than females C-LTMRs. We thus favor the hypothesis that this male-specific gene dysregulation non-cell-autonomously affects the signaling pathways responsible for GABA synthesis, transport, or release in GABAergic interneurons. Interestingly, typically nociceptor-specific genes such as *calca* (CGRP) and *Mrgprd* were among the 10 most upregulated genes in *bhlha9* KO male C-LTMRs (log2 fold change: 2.71 and 2.68 respectively, see Table S1). This could suggest a switch in their molecular profile to a more nociceptor-like identity. Moreover, the level of *penk* mRNA, which is the precursor of Leu- and Met-enkephalin, was found to be downregulated in those same FACS-sorted male CLTMRs (Figure 4E). It has been shown that mice lacking the voltage-gated sodium channel $Na_v1.7$ develop congenital insensitivity to pain and show a drastic upregulation of PENK (Minett et al., 2015). PENK has also been proposed to decrease GABA content in the striatum (Bernay et al., 2009). Based on these data, it is tempting to postulate that loss of BHLHA9 leads to decreased PENK secretion, which in turn contributes to the increase of GABA in GABAergic interneurons in our mice. Figure S3V shows that GABA content also increases in V1 terminals of GABAergic interneurons contacting $GINIP^+/VGLUT3^-$ and $GINIP^-/VGLUT3^-$ terminals. Our quantitative expression data (Figure S1A) and recently published RNA-sequencing data (Reynders et al., 2015; Usoskin et al., 2015) show that *bhlha9* can also be found in few other subpopulations of dorsal root ganglia neurons also known to form type Ia glomeruli in laminae II inner of dorsal SC.

In conclusion, our study adds an additional layer of knowledge to the growing literature on C-LTMRs. In particular, it shows for the first time that C-LTMR's contribution to modulation of formalin-evoked pain and the discriminative aspects of temperature sensation is sexually dimorphic and occurs through a fine regulation of spinal ionotropic GABAergic signaling. Whether ionotropic GABAergic regulation occurs cell autonomously or not is still an open question.

STAR★METHODS

Detailed methods are provided in the online version of this paper and include the following:

- KEY RESOURCES TABLE
- LEAD CONTACT AND MATERIALS AVAILABILITY
- EXPERIMENTAL MODEL AND SUBJECT DETAILS
  - Mice
- METHOD DETAILS
  - Histology
  - qRT-PCR
  - Behavioral assays
  - Thermal sensitivity
  - Hot plate
  - Cold plate
  - Thermal Gradient test
  - Two-temperature choice tests
  - Thermal nociceptive threshold (Hargreaves's test)
  - Mechanical sensitivity testing
  - Chemical sensitivity testing
  - Electron Microscopy (EM)
  - EM embedding
  - EM post-embedding immunostaining
  - Electrophysiological recording
  - FACS-sorting
  - RNA-seq analyses
- QUANTIFICATION AND STATISTICAL ANALYSIS
  - Neuronal counts and statistical analysis
  - EM quantification and statistical analysis
- DATA AND CODE AVAILABILITY

SUPPLEMENTAL INFORMATION

Supplemental Information can be found online at https://doi.org/10.1016/j.celrep.2019.12.041.

ACKNOWLEDGMENTS

We are grateful to the Moqrich lab members for fruitful scientific discussions. This work has been funded by the European Research Council (ERC) starting grant paineurons 260435 and the Agence Nationale de la Recherche (ANR) Myochronic to A.M. M.B.'s PhD thesis was funded by the Ministère de l'éducation nationale et de la recherche and la Fondation pour la recherche médicale (FRM). N.B.-A was supported by the Israel Science Foundation (1051/15).

AUTHOR CONTRIBUTIONS

A.M., I.M., and M.B. conceived the project and designed the experiments. M.B. performed most of the molecular, histological, and behavioral experiments; C. Salio performed the injury-induced mechanical pain experiments; N.B.-A. provided the Bhlha9 KO mice; P.M. managed the mouse colony for the FACS and electron microscopy experiments during the revision process; C. Santos performed all the immuno-EM and ultrastructural studies; A.R. performed FACS of C-LTMRs and RNA preparation for RNA sequencing and contributed to some *in situ* hybridization experiments; Y.L.F. performed electrophysiological experiments on SC neurons; A.J.S. analyzed all the RNA-sequencing data; and A.M. and M.B. co-wrote the manuscript.

DECLARATION OF INTERESTS

The authors declare no competing interests.

Received: December 12, 2018
Revised: November 18, 2019
Accepted: December 12, 2019
Published: January 21, 2020

REFERENCES

Ackerley, R., Carlsson, I., Wester, H., Olausson, H., and Backlund Wasling, H. (2014). Touch perceptions across skin sites: differences between sensitivity, direction discrimination and pleasantness. Front. Behav. Neurosci. *8*, 54.

Bennett, G.J., and Xie, Y.K. (1988). A peripheral mononeuropathy in rat that produces disorders of pain sensation like those seen in man. Pain *33*, 87–107.

Bernay, B., Gaillard, M.C., Guryca, V., Emadali, A., Kuhn, L., Bertrand, A., Detraz, I., Carcenac, C., Savasta, M., Brouillet, E., et al. (2009). Discovering new bioactive neuropeptides in the striatum secretome using in vivo microdialysis and versatile proteomics. Mol. Cell. Proteomics *8*, 946–958.

Brenner, D.S., Golden, J.P., and Gereau, R.W. (2012). A novel behavioral assay for measuring cold sensation in mice. PLoS One *7*, e39765.

Chaplan, S.R., Bach, F.W., Pogrel, J.W., Chung, J.M., and Yaksh, T.L. (1994). Quantitative assessment of tactile allodynia in the rat paw. J Neurosci Methods *53*, 55–63.

Delfini, M.C., Mantilleri, A., Gaillard, S., Hao, J., Reynders, A., Malapert, P., Alonso, S., François, A., Barrere, C., Seal, R., et al. (2013). TAFA4, a chemokine-like protein, modulates injury-induced mechanical and chemical pain hypersensitivity in mice. Cell Rep. *5*, 378–388.

Francois, A., Schuetter, N., Laffray, S., Sanguesa, J., Pizzoccaro, A., Dubel, S., Mantilleri, A., Nargeot, J., Noel, J., Wood, J.N., et al. (2015). The low-threshold calcium channel Cav3.2 determines low-threshold mechanoreceptor function. Cell Rep. *10*, 370–382.

Gaillard, S., Lo Re, L., Mantilleri, A., Hepp, R., Urien, L., Malapert, P., Alonso, S., Deage, M., Kambrun, C., Landry, M., et al. (2014). GINIP, a Galphai-Interacting Protein, Functions as a Key Modulator of Peripheral GABAB Receptor-Mediated Analgesia. Neuron *84*, 123–136.

Kambrun, C., Roca-Lapirot, O., Salio, C., Landry, M., Moqrich, A., and Le Feuvre, Y. (2018). TAFA4 reverses mechanical allodynia through activation of GABAergic transmission and microglial process retraction. Cell Rep. *22*, 2886–2897.

Kaneko, M., and Hammond, D.L. (1997). Role of spinal gamma-aminobutyric acidA receptors in formalin-induced nociception in the rat. J. Pharmacol. Exp. Ther. *282*, 928–938.

Li, L., Rutlin, M., Abraira, V.E., Cassidy, C., Kus, L., Gong, S., Jankowski, M.P., Luo, W., Heintz, N., Koerber, H.R., et al. (2011). The functional organization of cutaneous low-threshold mechanosensory neurons. Cell *147*, 1615–1627.

Liao, Y., Smyth, G.K., and Shi, W. (2013). The Subread aligner: fast, accurate and scalable read mapping by seed-and-vote. Nucleic acids research *41*, e108.

Liljencrantz, J., and Olausson, H. (2014). Tactile C fibers and their contributions to pleasant sensations and to tactile allodynia. Front. Behav. Neurosci. *8*, 37.

Löken, L.S., Evert, M., and Wessberg, J. (2011). Pleasantness of touch in human glabrous and hairy skin: order effects on affective ratings. Brain Res. *1417*, 9–15.

Love, M.I., Huber, W., and Anders, S. (2014). Moderated estimation of fold change and dispersion for RNA-seq data with DESeq2. Genome Biol. *15*, 550.

Minett, M.S., Pereira, V., Sikandar, S., Matsuyama, A., Lolignier, S., Kanellopoulos, A.H., Mancini, F., Iannetti, G.D., Bogdanov, Y.D., Santana-Varela, S., et al. (2015). Endogenous opioids contribute to insensitivity to pain in humans and mice lacking sodium channel Nav1.7. Nat. Commun. *6*, 8967.

Moqrich, A., Hwang, S.W., Earley, T.J., Petrus, M.J., Murray, A.N., Spencer, K.S., Andahazy, M., Story, G.M., and Patapoutian, A. (2005). Impaired thermosensation in mice lacking TRPV3, a heat and camphor sensor in the skin. Science *307*, 1468–1472.

Munro, G., Erichsen, H.K., Rae, M.G., and Mirza, N.R. (2011). A question of balance–positive versus negative allosteric modulation of GABA(A) receptor subtypes as a driver of analgesic efficacy in rat models of inflammatory and neuropathic pain. Neuropharmacology *61*, 121–132.

Nagi, S.S., Rubin, T.K., Chelvanayagam, D.K., Macefield, V.G., and Mahns, D.A. (2011). Allodynia mediated by C-tactile afferents in human hairy skin. J. Physiol. *589*, 4065–4075.

Nordin, M. (1990). Low-threshold mechanoreceptive and nociceptive units with unmyelinated (C) fibres in the human supraorbital nerve. J. Physiol. *426*, 229–240.

Reynders, A., and Moqrich, A. (2015). Analysis of cutaneous MRGPRD free nerve endings and C-LTMRs transcriptomes by RNA-sequencing. Genom. Data *5*, 132–135.

Ranade, S.S., Woo, S.H., Dubin, A.E., Moshourab, R.A., Wetzel, C., Petrus, M., Mathur, J., Begay, V., Coste, B., Mainquist, J., et al. (2014). Piezo2 is the major transducer of mechanical forces for touch sensation in mice. Nature *516*, 121–125.

Reynders, A., Mantilleri, A., Malapert, P., Rialle, S., Nidelet, S., Laffray, S., Beurrier, C., Bourinet, E., and Moqrich, A. (2015). Transcriptional profiling of cutaneous MRGPRD free nerve endings and C-LTMRs. Cell Rep. *10*, 1007–1019.

Salio, C., Lossi, L., Ferrini, F., and Merighi, A. (2005). Ultrastructural evidence for a pre- and postsynaptic localization of full-length trkB receptors in substantia gelatinosa (lamina II) of rat and mouse spinal cord. Eur J Neurosci *22*, 1951–1966.

Schatz, O., Langer, E., and Ben-Arie, N. (2014). Gene dosage of the transcription factor Fingerin (bHLHA9) affects digit development and links syndactyly to ectrodactyly. Hum. Mol. Genet. *23*, 5394–5401.

Seal, R.P., Wang, X., Guan, Y., Raja, S.N., Woodbury, C.J., Basbaum, A.I., and Edwards, R.H. (2009). Injury-induced mechanical hypersensitivity requires C-low threshold mechanoreceptors. Nature *462*, 651–655.

Urien, L., Gaillard, S., Lo Re, L., Malapert, P., Bohic, M., Reynders, A., and Moqrich, A. (2017). Genetic ablation of GINIP-expressing primary sensory neurons strongly impairs Formalin-evoked pain. Sci. Rep. *7*, 43493.

Usoskin, D., Furlan, A., Islam, S., Abdo, H., Lonnerberg, P., Lou, D., Hjerling-Leffler, J., Haeggstrom, J., Kharchenko, O., Kharchenko, P.V., et al. (2015). Unbiased classification of sensory neuron types by large-scale single-cell RNA sequencing. Nat. Neurosci. *18*, 145–153.

Vallbo, A.B., Olausson, H., and Wessberg, J. (1999). Unmyelinated afferents constitute a second system coding tactile stimuli of the human hairy skin. J. Neurophysiol. *81*, 2753–2763.

Zimmermann, K., Hein, A., Hager, U., Kaczmarek, J.S., Turnquist, B.P., Clapham, D.E., and Reeh, P.W. (2009). Phenotyping sensory nerve endings in vitro in the mouse. Nat. Protoc. *4*, 174–196.

Zotterman, Y. (1939). Touch, pain and tickling: an electro-physiological investigation on cutaneous sensory nerves. J. Physiol. *95*, 1–28.

STAR★METHODS

KEY RESOURCES TABLE

REAGENT or RESOURCE	SOURCE	IDENTIFIER
Antibodies		
Rat anti-GINIP	Gaillard et al., 2014	N/A
Goat anti-TrkC	R&D Systems	Cat# AF1404, RRID:AB_2155412
Rabbit anti-CGRP	Chemicon	Cat# PC205L-100UL, RRID:AB_564312
Rabbit anti-PKCg	Santa Cruz Biotechnology	Cat# sc-211, RRID:AB_632234
Rabbit anti-S100	Dako	Cat# GA50461-2, RRID:AB_2811056
Rabbit anti-VGLUT3	Abcam	Cat# ab23977 RRID:AB_2270290
Mouse anti-GABA	Sigma	Cat# A0310 RRID:AB_476667
Chemicals, Peptides, and Recombinant Proteins		
NS11394	MedChem Express	CAS No.: 951650-22-9
Critical Commercial Assays		
RNeasy Micro Kit	Quiagen	https://www.qiagen.com/us/products/
RNA Pico Chip	Agilent	http://www.integratedsci.com.au/product/rna-6000-pico-kit-and-reagents.html
Deposited Data		
Raw data	This paper	GEO: GSE138245
Experimental Models: Organisms/Strains		
Mouse: bHLHa9-lacZ	Schatz et al., 2014	N/A
Mouse: Tafa4-Venus	Delfini et al., 2013	N/A
Software and Algorithms		
ImageJ		https://imagej.nih.gov/ij/
Graph Pad Prism 6	GraphPad software, San Diego, CA	https://www.graphpad.com/scientific-software/prism/
Zen Blue	Carl Zeiss, Germany	https://www.zeiss.com/microscopy/int/products/microscope-software/zen.html
Thermal Gradient Test software	Bioseb	https://www.bioseb.com/bioseb/anglais/default/software.php
DESeq2	Love, Huber, and Anders 2014	https://bioconductor.org/packages/release/bioc/html/DESeq2.html

LEAD CONTACT AND MATERIALS AVAILABILITY

Further information and requests for resources and reagents should be directed to and will be fulfilled by the Lead Contact Aziz Moqrich (aziz.moqrich@univ-amu.fr). This study did not generate new unique reagents.

EXPERIMENTAL MODEL AND SUBJECT DETAILS

Mice

Male and female wild-type and bhlha9 KO mice were generated from heterozygous crosses. They were maintained under standard housing conditions (22°C, 40% humidity, 12 h light cycles, and free access to food and water). Special effort was made to minimize the number as well as the stress and suffering of mice used in this study. All procedures were conducted according to the French Ministry of Agriculture and the European Community Council Directive no 2015070217242262-V5#1537

METHOD DETAILS

Histology

In situ hybridization and immunofluorescence

In situ hybridization and immunofluorescence were performed following standard protocols (Li et al., 2011; Reynders et al., 2015).

To obtain adult DRG and spinal cord, mice were deeply anesthetized with a mix of ketamine/xylazine and then transcardially perfused with an ice-cold solution of paraformaldehyde 4% in PBS (PAF). After dissection, DRG were postfixed for at least 2 to 24 h in the same fixative at 4°C. Tissues were then transferred into a 30% (w/v) sucrose solution for cryoprotection before being frozen and stored at −80°C. Samples were sectioned (12 to 40 μm) using a standard cryostat (Leica). RNA probes (bhlha9, TrkA, TrkB, Ret) were synthesized using gene-specific PCR primers and cDNA templates from adult mouse DRG.

In situ hybridization was performed using digoxigenin labeled probes. Probes were hybridized overnight at 55°C, and the slides incubated with the horseradish peroxidase anti-digoxigenin antibody (Roche). Final detection was achieved using cy3 TSA plus kit (Perkin Elmer). The following oligonucleotides were used for nested PCRs for probe synthesis:

bhlha9-F1: AACCGGGCTGAGGATTTTGT,
bhlha9-R1: CCACGAAACCGGTCGAACA,
bhlha9-F2: TTTTGTGGAGGACTTGGGGC,
bhlha9-R2+T7: TAATACGACTCACTATAGGGGACATTGACGCCAGTTTCCC,
TrkA-F1: TTTGCTCTCCTCTCATCTCTCC,
TrkA-R1: AAATTGATTCCAGAGACCCAGA,
TrkA-F2: GGCGATCGAGTGTATCACG,
TrkA-R2+T7: TAATACGACTCACTATAGGGTAATTGCTATTATGATGGATGCTG,
TrkB-F1: CTGAGAGGGCCAGTCACTTC,
TrkB-R1: CATGGCAGGTCAACAAGCTA,
TrkB-F2: CAGTGGGTCTCAGCACAGAA,
TrkB-R2+T7: TAATACGACTCACTATAGGGCTAGGACCAGGATGGCTCTG,
Ret-F1: TTAGATCCCCTTTCCCTTTAGC,
Ret-R1: GAGTGTCTGTGGCTACAACTGC,
Ret-F2: CTGCTCATCACTAGCCACCA,
Ret-R2+T7: TAATACGACTCACTATAGGGTGTGCCTTTCACACAAGCTC

For immunofluorescence, primary antibodies were diluted in PBS - 10% donkey or goat serum (Sigma) - 3% bovine albumin (Sigma) - 0.4% Triton X-100 and incubated overnight at 4°C. Primary antibodies used in this study are as follows: goat anti-TrkC 1:1000 (R&D Systems), rabbit anti-CGRP 1:1000 (Chemicon), rabbit anti-PKCγ 1:1000 (Santa Cruz Biotechnology), rabbit anti-S100 1:400 (Dako), rat anti-GINIP 1:1000 (generated in the lab,; Gaillard et al., 2014). Corresponding donkey or goat anti-rabbit, anti-rat, and anti-goat Alexa 488, 555, or 647 (Invitrogen or Molecular probe antibodies) were used for secondary detection. Isolectin IB4 Conjugated to Alexa Fluor 488 dye was used at 1:200 (Invitrogen).

For whole mount skin immunostaining as described in (Li et al., 2011), back hairy skin was shaved using a commercial hair remover, wiped clean with PBS and tissue, tape stripped and dissected. Excess fat and skin was removed, the remaining tissue cut in small pieces and fixed with 4% PAF at 4°C for 2h, rinsed with PBS then washed with PBS+0.3% triton every 30 min for 6h at room temperature (RT). Tissue incubation with primary antibodies was done over 3 days at RT in PBS+0.3% Triton + 5% Donkey serum + 20% DMSO. Tissues were washed with PBS+0.3% Triton every 30 min for 6h at RT, incubated with secondary antibodies for 4 days at RT in PBS+ 0.3% Triton + 5% Donkey serum + 20% DMSO, washed with PBS+0.3% Triton every 30 min for 6h at RT, dehydrated in 50% methanol for 5 min at RT, then in 100% methanol for 20 min at RT and finally cleared in BABB (benzyl alcohol + benzyl benzoate 1:2) for 20 min at RT.

qRT-PCR

Thoracic pairs of DRGs were dissected from P1, P8, P14, P20 and adult WT male mice. Cerebellum, hippocampus and cortex were dissected from adult WT male mice. RNA was extracted by using the RNeasy Mini Kit (Quiagen), according to manufacturer's instructions. RNA samples were reverse-transcribed into cDNA (ImpromII Reverse Transcriptase, Promega) and used as template for qRT-PCR quantification of bhlha9 expression using the following oligos:

Fw: GCATCCTGGATTACAACGAGGC,
Rv: CAAGGATAGAGCAGTGATGCGG.

Behavioral assays

All behavioral assays were conducted on WT and bhlha9 KO littermates of 8-12 weeks in age. Animals were acclimated for 30 min to their testing environment prior to all experiments that are done at room temperature (~22°C). Experimenters were blind to the genotype of the mice during testing. Students' t test was used for all statistical calculations. All error bars represent standard error of the mean (SEM). General behavioral (Locomotor and learning activity) was measured using Rotarod apparatus (LSI Letica Scientific Instruments). Gradient, Thermal plates, open field, Hargreaves and Von Frey apparatus were from Bioseb instruments.

General behavioral assays

Thermal sensitivity

Response to temperature choice test and Response to temperature Gradient assay were performed as described in (Moqrich et al., 2005) but using Bioseb apparatus.

Hot plate

To assess heat sensitivity, mice were confined individually to a metal surface maintained at 48°C, 50°C, 52°C and 55°C by a Plexiglas cylinder 20 cm high, and the latency to nociceptive responses (licking, shaking or jumping of hind paws) measured. To prevent tissue damage, mice were removed from the plate immediately after a nociceptive response or after a maximum of 90 s, 60 s, 45 s and 20 s respectively. Each mouse has been tested three times at 48°C, 50°C and 52°C and twice at 55°C with a latency of 5 min between each test; the withdrawal time corresponds to the mean of all measures. A latency of at least 1h between each tested temperature was respected.

Cold plate

This test was performed as described by Brenner and colleagues (Brenner et al., 2012). To test cold sensitivity, mice were allowed to acclimate on a glass plate, placed individually in plastic chambers for 1 hour. Then crushed dry ice, piled in a syringe with the tip cut-off, was applied right under the middle of the hindpaw of the mouse. We measured the latency until lifting of the paw with a cut-off of 20 s to avoid tissue damage. Each mouse was exposed six times with a minimum of 5 min resting period between trials. In the case of the cold test following CCI, Figure S2F show the result of stimulation of the injured hindpaw.

Thermal Gradient test

This test has been described previously (Moqrich et al., 2005). Briefly, mice were individually tracked for 90 min in four separate arenas of the thermal gradient apparatus (Bioseb). A controlled and stable temperature gradient of 14°C to 53.5°C was maintained using two Peltier heating/cooling devices positioned at each end of the aluminum floor. Each arena was virtually divided into 15 zones of equal size (8 cm) with a distinct and stable temperature. The tracking was performed using a video camera controlled by the software provided by the manufacturer.

Two-temperature choice tests

Two mice were placed simultaneously in each lane of the two temperature choice apparatus (Bioseb). Mice were tracked for 10 min using the Bioseb software. During the first day, both plates were kept at 20°C during 10 min. Days after this acclimatizing period, 2 plates were individually warmed or cooled to different temperature (42°C to 16°C) and kept at the appropriate temperature for 10 min test. A 1h time lapse was respected between 2 different tests.

Thermal nociceptive threshold (Hargreaves's test)

To assess hindpaw heat sensitivity, Hargreaves' test was conducted using a plantar test device (Bioseb). Mice were placed individually into Plexiglas chambers on an elevated glass platform and allowed to acclimate for at least 30 min before testing. A mobile radiant heat source of constant intensity was then applied to the glabrous surface of the paw through the glass plate and the latency to paw withdrawal measured. Paw withdrawal latency is reported as the mean of three measurements for both hindpaws with at least a 5 min pause between measurements. IR source was adjusted to 20% and a cut-off of 20 s was applied to avoid tissue damage.

Mechanical sensitivity testing

Tape Response Assay

This test was performed as described by Ranade and colleagues (Ranade et al., 2014). Briefly, mice were allowed to put in a Plexiglas cylinder and allowed to acclimate for 5 min; a piece of 3 cm of tape was gently applied to the back of the mouse. Mice were then observed for 5 min and the total number of responses to the tape was counted. A response was scored when the mouse stopped moving and bit or scratched the piece of tape or showed a visible "wet dog shake" motion in an attempt to remove the foreign object on its back.

Von frey filaments test

Mice were placed in plastic chambers on a wire mesh grid and stimulated with von Frey filaments (Bioseb) using the up-down method (Chaplan et al., 1994) starting with 1g and ending with 2g filament as cut-off value.

Chemical sensitivity testing

Formalin test

Formalin solution was prepared at 2% in PBS 1X from a formalin stock (Fischer Scientific) (note that formalin stock corresponds to a 37% formaldehyde solution). Mice were placed individually into Plexiglas chambers, allowed to habituate to the testing environment for 30 min. Following subcutaneous injection of 10 μL of formalin for a mouse weighing 25 g in the left hind paw, the animals were immediately placed individually in observation chambers and then monitored for pain behavior (shaking, licking, and biting of the

injected paw) for 60 min. The pain behavior cumulative time of the injected paw was counted at 5 min intervals. Time spent exhibiting these pain behaviors was recorded for the first phase (0-10 min) and the second phase (10-60 min).

Administration of PAM

NS11394 was dissolved in 5% Tween80/milliQ water as adapted from (Munro et al., 2011). Mice were administered per os with NS11394 (MedChem Express) 30 min prior to formalin injection just before being allowed to habituate to the Plexiglas cylinder. The dosing volumes were 1 and 3 mg/kg with an average mouse weighing 25 g being administered 250 μL and later injected with 10 μL of formalin.

Carrageenan injection

20 μL of 1% λ -Carrageenan (Sigma-Aldrich, 22049-5G-F) in PBS 1X was injected into the mouse left hind paw using a Hamilton syringe. For the Carrageenan model, mechanical allodynia and hyperalgesia were assessed before and after injection using the up-down method starting with the 1g Von Frey hair filament and ending with the 2g filament as cut-off value. The uninjected right hind-paw served as a control.

Unilateral peripheral mononeuropathy

For the chronic constriction of the sciatic nerve (CCI) model, unilateral peripheral mononeuropathy was induced in mice anaesthetized with Ketamine (40mg/kg ip) and Xylasine (5mg/kg ip) with three monocryl (6/0, Ethicon) ligatures tied loosely (with about 1mm spacing) around the common sciatic nerve (Bennett and Xie, 1988). The nerve was constricted to a barely discernible degree, so that circulation through the epineurial vasculature was not interrupted.

For the chronic constriction model, mechanical allodynia, and hyperalgesia were assessed before the surgery and every other 7 days' post-surgery using the up-down method starting with the 1g Von Frey hair filament and ending with the 2g filament as cut-off value. The uninjured right hind-paw served as a control.

Electron Microscopy (EM)

Tissue preparation for ultrastructural morphology

WT (n = 3 females; n = 3 males) and Bhlha9 KO mice (n = 2 females; n = 3 males) were deeply anesthetized with sodium pentobarbital (60mg/100 g) and perfused with Ringer solution followed by 1% PAF + 2% glutaraldehyde in 0.1 M phosphate buffer, pH 7.4. Lumbar spinal cord segments were dissected out and postfixed for 2 h in the same aldehyde mixture. Coronal sections were cut on a vibratome (Leica VT1000S) at a thickness of 80 μm.

EM embedding

Spinal cord sections were post-fixed in osmium ferrocyanide for 1 h at 4°C, dehydrated in graded acetone, incubated in acetone/Spurr resin (1:1; 30 min), acetone/Spurr resin (1:2; 30 min) and Spurr resin overnight at room temperature. Finally, sections were flat-embedded in Spurr resin (24 h, at 70°C). Ultrathin sections were cut with an ultramicrotome (EM UC6, Leica) and collected on uncoated nickel grids (200 mesh).

EM post-embedding immunostaining

Ultrathin sections were triple immunostained following a conventional post-embedding protocol (Salio et al., 2005). Sections were treated for 2 min with a saturated aqueous solution of sodium metaperiodate (Sigma), rinsed in 1% Triton X-100 in Tris buffered saline (TBS) 0.5 M, and incubated for 1 h in 10% normal serum. Grids were then incubated overnight on drops of a mixture of primary antibodies at optimal dilutions. After rinsing in TBS, they were incubated in a mixture of the appropriate secondary antibodies gold conjugates (1:15; BBI Solutions, Cardiff, United Kingdom). They were then transferred into drops of 2.5% glutaraldehyde in cacodylate buffer 0.05 M pH 7.4 for 10 min, and finally washed in distilled water. Sections were further counterstained for 30'' with Uranyl Less EM Stain and for 30'' with Lead citrate (Electron Microscopy Sciences, Hatfield, PA, USA).

Sections were observed with a JEM-1010 transmission electron microscope (Jeol, Tokyo, Japan) equipped with a side-mounted CCD camera (Mega View III, Olympus Soft Imaging System, Brandeburg, Germany).

The following primary antibodies were used for EM immunostaining: rat anti-GINIP (1:20, Gaillard et al., 2014; Salio et al., 2005), rabbit anti-VGLUT3 (1:10, Abcam, Cat# ab23977 RRID: AB_2270290), mouse anti-GABA (1:50; Sigma, Cat# A0310 RRID:AB_476667). Routine immunohistochemical controls consisted in omission of primary antibodies.

Electrophysiological recording

Transverse spinal cord slices with attached dorsal roots from juvenile (P24 to P45) bhlha9 KO and WT mice were prepared for whole-cell recording. Briefly, the animals were anesthetized using Pentobarbital (200 mg/kg), perfused with ice cold oxygenated sodium free artificial cerebrospinal fluid (ACSF; in mM: ClCholine 101; KCl 3.8; $MgCl_2$ 18.7; $MgSO_4$ 1.3; KH_2PO_4 1.2; HEPES 10; $CaCl_2$ 1; Glucose 1), and then beheaded. The vertebral column and surrounding muscles were quickly removed and immersed in ice cold oxygenated ACSF. Following laminectomy, the spinal cord was gently removed and its lumbar part was placed into a small 3% agarose block. Spinal slices (300 μm thick) were cut using a Leica VTS1000 vibratome, and transferred in warm (31°C) ACSF (in mM: NaCl 130.5; KCl 2.4; $CaCl_2$ 2.4; $NaHCO_3$ 19.5; $MgSO_4$ 1.3;KH_2PO_4 1.2; HEPES 1.25; glucose 10; pH 7.4) equilibrated with 95%O_2-5%CO_2 for

at least one h before starting patch clamp recordings. Spinal slices were placed in a recording chamber bathed with warmed (31°C) ACSF Electrophysiological measurements were performed under the control of an Olympus BX51 microscope using a multiclamp 2B (Molecular devices). Patch pipettes (7-11 Ω) were filled with potassium gluconate-based pipette solution (in mM: Potassium D-Gluconate 120; KCl 20; $CaCl_2$ 0.1; $MgCl_2$ 1.3; EGTA 1; HEPES 10; GTP 0.1; cAMP 0.2; Leupeptin 0.1; Na_2ATP 3; D-Manitol 77; pH 7.3). All drugs were purchased from Sigma. Synaptic analysis was performed using Spike 2 software and at least 3 min of recordings were used to quantify EPSC parameters. Sag ratio was calculated as the difference between steady-state (Vss) and peak-voltage (Vp) variations during a hyperpolarizing current pulse (ratio = (Vss-Vp)/Vp) and IO rectification was calculated by dividing the slope of the current response curve at −60mV and −100mV (IOrect = [(dI/dV-60) / (dI/dV-100)]). For each cell, an average EPSC was calculated and the kinetics of these averaged EPSCs were compared between WT and KO animals. One-way ANOVA was used to assess for differences in cells intrinsic and synaptic properties in the WT and KO males and females. Effects of NS11394 on EPSC frequency and amplitude was assessed for each cell using Kolmogorov Smirnov test, and paired t test was used to assess the effect of NS1134 within each group.

FACS-sorting

Thoracic and lumbar DRG from WT::Tafa4venus/+ and bhlha9 KO::Tafa4venus/+ mice were dissected and cell suspensions were prepared as previously described (Reynders et al., 2015; Reynders and Moqrich, 2015). C-LTMRs were sorted on FACS Aria (BD Bioscience) by gating on Sytox red- (live cells) GFP+ cells. For each biological replicate of WT and bhlha9 KO males and females, 3 to 5 mice were pooled per genotype and gender.

RNA-seq analyses

Total RNA was extracted from FACS-sorted C-LTMRs from biological replicates of adult WT and bhlha9 KO males and females using RNeasy Micro Kit (Quiagen), according to manufacturer's instructions. For quality control RNAs were loaded on a RNA Pico Chip (Agilent) and processed with 2100 Bioanalyzer system (Agilent technology). Full-length cDNA was generated from 500 pg of total RNA using Clontech SMART-Seq v4 Ultra Low Input RNA kit for Sequencing (Takara Bio Europe, Saint Germain en Laye, France) according to manufacturer's instructions with 13 cycles of PCR for cDNA amplification by Seq-Amp polymerase. Six hundreds pg of pre-amplified cDNA were then used as input for Tn5 transposon tagmentation by the Nextera XT DNA Library Preparation Kit (96 samples) (Illumina, San Diego, CA) followed by 12 cycles of library amplification. Following purification with Agencourt AMPure XP beads (Beckman-Coulter, Villepinte, France), the size and concentration of libraries were assessed by capillary electrophoresis.

Following sequencing (HiSeq 4000, Illumina, San Diego, CA) using a 100-nt paired-end read protocol (65-82 x106 reads per sample), sequences were mapped to the mm10 UCSC mouse genome assembly resulting in 91%–93% correctly mapped reads, which were used for differential gene expression analyses. Raw counts from mapped reads mapping to mm10 exons were obtained using featureCounts from the Subread package (Liao et al., 2013) (Version 1.6.1). Differentially expressed genes were called using DESeq2 (Love et al., 2014) (version 1.14.1) using a false discovery rate (p-adjusted value in DESeq2) threshold of 0.05 and at least a two-fold change in expression.

QUANTIFICATION AND STATISTICAL ANALYSIS

Neuronal counts and statistical analysis

12 μm serial sections of thoracic (T12) DRGs were distributed on six slides and subjected to different markers including the pan-neuronal marker SCG10. This approach allowed us to represent all counts as percentage of the total number of neurons (SCG10+). For each genotype, two DRGs were counted in at least three independent mice. Statistical significance was set to $p < 0.05$ and assessed using one-way ANOVA followed by unpaired t test.

EM quantification and statistical analysis

To assess whether loss-of-function of bhlha9 affects C-LTMR central terminals organized in non-peptidergic type Ia glomeruli (GIa) and synaptic contacts, a quantitative analysis was performed in lamina II as follows: (i) counting of GIa, immunolabeled or not for GINIP and/or VGLUT3 in WT versus KO male and female mice; (ii) counting of GABA-immunolabeled vesicle-containing dendrites (V1) engaged in the GIa glomerular configuration in WT versus KO male and female mice.

A total of 10 randomly selected sections/animal for WT (males and females) and bhlha9 (females and males) mice were examined and quantification was directly performed on ultrathin sections within 90x90 m squares of 200 mesh EM grids by an operator blinded to the experimental groups. Quantitative and statistical analyses were performed by using ImageJ software (NIH, Bethesda, USA) and Graph Pad Prism 6 (GraphPad software, San Diego, CA).

The number of GIa/area (N/2) was counted after GIa identification with well-established criteria (Ribeiro-da-Silva, 2004) and the percentages of GINIP+/VGLUT3+, GINIP+/VGLUT3- and GINIP-/VGLUT3- GIa were calculated. GIa density was evaluated with ordinary one-way analysis of variance (ANOVA) test and differences were considered significant for $p < 0.05$.

For quantification of GABA immunolabeling the number of gold particles (GPs) over V1 profiles engaged in GIa configuration (GPs/area; N/2) was calculated. The density of GPs over resin was chosen as an index of background (bk) staining and determined for each animal by calculating the mean GP density value over 10 randomly selected sections. Being the bk values of the four experimental

groups not statistically different when analyzed with ordinary one-way ANOVA and thus indicating independence from the experimental group, the bk mean value of the four groups was used as bk index. Differences in GABA immunolabeling were evaluated with non-parametric Mann Whitney test, since preliminary Shapiro test have proven that data were not normally distributed. Differences were considered significant for $p < 0.05$.

DATA AND CODE AVAILABILITY

The RNA-seq data have been deposited in NCBI's Gene Expression Omnibus and are accessible through GEO Series accession number GSE138245.